Large-scale shell-model calculations of nuclear Schiff moments of ^{129}Xe and ^{199}Hg

Kota Yanase* and Noritaka Shimizu†
Center for Nuclear Study, the University of Tokyo, 7-3-1 Hongo, Bunkyo-ku, Tokyo, Japan

(Received 2 July 2020; revised 14 September 2020; accepted 7 December 2020; published 30 December 2020)

The theoretical uncertainty in the nuclear Schiff moment is an obstacle to set constraints on charge-parity violation beyond the standard model from experimental upper bounds on atomic electric dipole moments. We perform large-scale shell-model calculations of the ^{129}Xe and ^{199}Hg nuclei with realistic effective interactions. To estimate the Schiff moments caused by the P, T-odd πNN interaction perturbatively, we employ the one-particle–one-hole approximation to the intermediate states. The Schiff moments of ^{129}Xe and ^{199}Hg are reduced due to the configuration mixing by $\sim$10% from the evaluation of the independent particle model. On the other hand, the reduction is more significant in mean-field based calculations and shell-model calculations with a drastic truncation. In order to resolve the discrepancy in the Schiff moment of ^{199}Hg among several nuclear models, we survey low-energy nuclear structure. The large-scale shell-model calculations reveal that the Schiff moment of ^{199}Hg is considerably quenched in the second $\frac{1}{2}^-$ state.

DOI: 10.1103/PhysRevC.102.065502

I. INTRODUCTION

The permanent electric dipole moments (EDMs) of atoms are expected as probes of charge-parity (CP) violation beyond the standard model. It is known that atomic EDMs are greatly enhanced by the relativistic effect of the electron EDM in alkali atoms [1,2] and paramagnetic atoms with similar configurations of electron [3]. It has been demonstrated by atomic many-body calculations that the enhancement factors are greater than 100 in the cesium, thallium, and francium atoms [4–7]. The experimental measurements of the cesium [8,9] and thallium atoms [10,11] presented upper bounds on the electron EDM. Recently, an experiment was proposed to measure the atomic EDM of francium in spite of its difficulty owing to the metastability of the nucleus [12]. Recent measurements using the thorium monoxide molecule improved the best limit on the electron EDM by orders of magnitude [13,14]. The current status is $|d_e| < 1.1 \times 10^{-29} e\,\mathrm{cm}$.

The CP violation due to the electron EDM must be suppressed in diamagnetic atoms because of the closed configurations of electron [15,16]. The EDMs of diamagnetic atoms are alternatively sensitive to the CP violation in atomic nuclei including the P, T-odd nucleon-nucleon (NN) interactions. The P, T-odd NN interactions induce nuclear EDMs, but those are completely screened in neutral atoms due to the interactions with surrounding electrons. One of the leading contributions to the EDM of a diamagnetic atom arises from the nuclear Schiff moment (NSM) induced by the P, T-odd NN interactions [17–19]. The experimental precision has been improved for a long time in ^{199}Hg [20–26] and ^{129}Xe [27–30]. In particular the ^{199}Hg atomic EDM is the most precise measurement among all the particles so far. The present constraint is $|d_{\mathrm{Hg}}| < 7.4 \times 10^{-30} e\,\mathrm{cm}$. Some actinide atoms are paid attentions in spite of experimental difficulties because octupole deformation of atomic nuclei is supposed to greatly enhance the NSMs [31,32]. The upper bound of the ^{225}Ra atomic EDM was first reported several years ago [33,34].

In the present study we concentrate on the ^{129}Xe and ^{199}Hg NSMs induced by the P, T-odd NN interactions. Most of the many-body calculations for those nuclei are based on the mean-field approximation so far. In early studies an independent particle model (IPM) is employed with the phenomenological Woods-Saxon potential and the spin-orbit correction [35,36]. Subsequently, the residual interactions were taken into account in the random phase approximation (RPA) and quasiparticle RPA (QRPA) [37–39]. They performed mean-field calculations in ^{198}Hg and added a neutron to describe the ground state of ^{199}Hg. Considering the P, T-odd πNN interaction, the isoscalar and isotensor channels are suppressed, whereas the isovector coefficient is still comparable with results of IPM calculations. However, fully self-consistent Hartree-Fock-Bogoliubov (HFB) calculations of ^{199}Hg itself presented controversial results [40]. Although the same Skyrme interactions with the QRPA calculations are employed, the effects of the residual interactions greatly reduce the isovector coefficient so as to change its sign. The authors inferred that the soft quadrupole deformation of the ^{199}Hg nucleus might give rise to the theoretical uncertainty and claimed the necessity of configuration mixing.

In the nuclear shell model, wave functions are expressed as linear combinations of the vast number of Slater determinants in the restricted valence space. In preceding studies, possible configurations were drastically truncated to evade the sizable numerical cost due to a number of active protons and neutron holes of ^{129}Xe [41,42]. That simplified version of the shell model is referred to as the pair-truncated shell model (PTSM), in which the many-body bases are composed of collective

*yanase@cns.s.u-tokyo.ac.jp
†shimizu@cns.s.u-tokyo.ac.jp

pairs of like nucleons. In the PTSM studies, schematic pairing plus quadrupole interactions were adopted. The RPA [38] and the PTSM [42] studies agree in that the NSM of ^{129}Xe is reduced roughly by one order of magnitude from the IPM results.

In this paper, we perform large-scale shell-model (LSSM) calculations of ^{129}Xe and ^{199}Hg utilizing realistic effective interactions based on the G-matrix interactions. The P, T-odd πNN interaction can be treated as a perturbation. As discussed in the following section, we adopt the one-particle–one-hole approximation to the intermediate states, where the residual correlations are neglected. A natural progression of the present study is to expand the valence space in the LSSM calculations.

II. FORMULATION

The electric dipole moment (EDM) of an atom is defined by

$$\boldsymbol{d}_{\rm atom} = -\sum_{i=1}^{Z} e\boldsymbol{r}_i, \tag{1}$$

where the summation runs over atomic electrons. The atomic EDM has a nonzero value only if P and T symmetries are both violated in the atomic system. The same argument is applicable to the nuclear Schiff moment (NSM), which requires P and T violations in the atomic nucleus. The NSM violates P and T symmetries of the atomic system through the interactions with electrons.

The NSM operator is defined by [43]

$$\boldsymbol{S} = \frac{e}{10}\sum_{i=1}^{Z}\left(r_i^2\boldsymbol{r}_i - \frac{5}{3}\langle r^2\rangle_{\rm ch}\boldsymbol{r}_i\right), \tag{2}$$

where $\boldsymbol{r}_i$ indicates the proton coordinates with the electric charge e, and $\langle r^2\rangle_{\rm ch}$ is the mean squared radius of the charge distribution. The NSM of a spin-J state is given by the expectation value in the largest projection $M = J$.

The NSM can be induced by the P, T-odd NN interactions. Considering the one-pion-exchange P, T-odd NN interaction, the nuclear Hamiltonian contains the following P, T-odd potential:

$$\begin{aligned}
\widetilde{V} &= \sum_{T=0,1,2}\widetilde{V}_T,\\
\widetilde{V}_0 &= F_0(\boldsymbol{\tau}_1\cdot\boldsymbol{\tau}_2)(\boldsymbol{\sigma}_1-\boldsymbol{\sigma}_2)\cdot\nabla\frac{e^{-m_\pi r}}{r},\\
\widetilde{V}_1 &= F_1[(\tau_{1z}+\tau_{2z})(\boldsymbol{\sigma}_1-\boldsymbol{\sigma}_2)\\
&\quad +(\tau_{1z}-\tau_{2z})(\boldsymbol{\sigma}_1+\boldsymbol{\sigma}_2)]\cdot\nabla\frac{e^{-m_\pi r}}{r},\\
\widetilde{V}_2 &= F_2(3\tau_{1z}\tau_{2z}-\boldsymbol{\tau}_1\cdot\boldsymbol{\tau}_2)(\boldsymbol{\sigma}_1-\boldsymbol{\sigma}_2)\cdot\nabla\frac{e^{-m_\pi r}}{r},
\end{aligned} \tag{3}$$

where $\boldsymbol{r} = \boldsymbol{r}_1 - \boldsymbol{r}_2$ is the relative coordinate of two nucleons and m_π denotes the pion mass. The subscripts $T = 0, 1, 2$ represent the isospin structures of the P, T-odd vertex $\bar{g}^{(T)}_{\pi NN}$. The other side of the P, T-odd πNN interaction must be the P, T-even vertex $g_{\pi NN}$. Those couplings are contained in

$$\begin{aligned}
F_0 &= \frac{1}{8\pi M_N}g_{\pi NN}\bar{g}^{(0)}_{\pi NN},\\
F_1 &= -\frac{1}{16\pi M_N}g_{\pi NN}\bar{g}^{(1)}_{\pi NN},\\
F_2 &= \frac{1}{8\pi M_N}g_{\pi NN}\bar{g}^{(2)}_{\pi NN},
\end{aligned} \tag{4}$$

where M_N denotes the nucleon mass.

In the infinite pion-mass limit, the one-pion-exchange P, T-odd NN interaction is related to the contact interaction [36,38,44]

$$\widetilde{V}_C = \frac{G}{\sqrt{2}}\frac{1}{2m_N}(\eta_{ab}\boldsymbol{\sigma}_a - \eta_{ba}\boldsymbol{\sigma}_b)\cdot\nabla\delta(\boldsymbol{r}), \tag{5}$$

where G is the Fermi coupling constant and

$$\begin{aligned}
\eta_{nn} &= \frac{\sqrt{2}}{Gm_\pi^2}g_{\pi NN}\left(\bar{g}^{(0)}_{\pi NN}+\bar{g}^{(1)}_{\pi NN}+2\bar{g}^{(2)}_{\pi NN}\right),\\
\eta_{pp} &= \frac{\sqrt{2}}{Gm_\pi^2}g_{\pi NN}\left(\bar{g}^{(0)}_{\pi NN}-\bar{g}^{(1)}_{\pi NN}+2\bar{g}^{(2)}_{\pi NN}\right),\\
\eta_{np} &= \frac{\sqrt{2}}{Gm_\pi^2}g_{\pi NN}\left(-\bar{g}^{(0)}_{\pi NN}+\bar{g}^{(1)}_{\pi NN}-2\bar{g}^{(2)}_{\pi NN}\right),\\
\eta_{pn} &= \frac{\sqrt{2}}{Gm_\pi^2}g_{\pi NN}\left(-\bar{g}^{(0)}_{\pi NN}-\bar{g}^{(1)}_{\pi NN}-2\bar{g}^{(2)}_{\pi NN}\right).
\end{aligned} \tag{6}$$

The exchange terms are not contained in the expression (5) since nuclear wave functions used in this paper are antisymmetrized. The contact P, T-odd NN interaction originated from the Weinberg operator could be as important as the P, T-odd πNN interaction at low energies [45].

The nuclear Hamiltonian is expressed as

$$H = H_0 + \widetilde{V}, \tag{7}$$

where H_0 denotes P, T-even NN interactions. Since the P, T-odd πNN interaction $\widetilde{V}$ should be very weak, the ground state of H is expressed without the normalization as

$$|\psi\rangle = |\psi_0\rangle + \sum_n \frac{|\psi_n\rangle\langle\psi_n|\widetilde{V}|\psi_0\rangle}{E_0 - E_n}, \tag{8}$$

where $|\psi_0\rangle$ is the ground state of H_0 and $|\psi_n\rangle$ denotes the excited states of the same $(J, M = J)$ and the opposite parity. The NSM is then calculated as

$$\begin{aligned}
\langle\psi|S_z|\psi\rangle &= \sum_n \frac{\langle\psi_0|S_z|\psi_n\rangle\langle\psi_n|\widetilde{V}|\psi_0\rangle}{E_0-E_n} + c.c.\\
&= \sum_{T=0}^{2} a_T g_{\pi NN}\bar{g}^{(T)}_{\pi NN},
\end{aligned} \tag{9}$$

where $c.c.$ denotes the complex conjugate. The numerical results on nuclear physics are put together in the coefficients a_T, which are referred to as NSM coefficients in this paper.

In order to obtain wave functions of the ground states in ^{129}Xe and ^{199}Hg, we perform large-scale shell-model (LSSM)

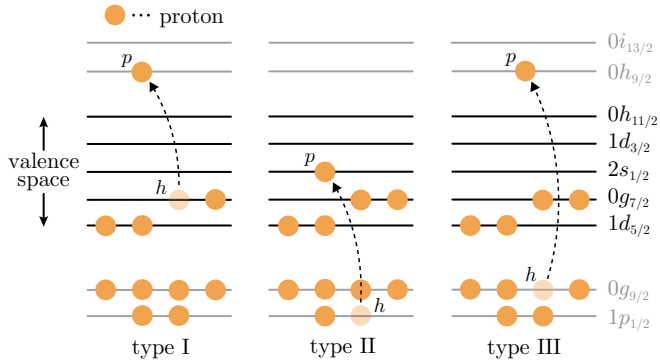

FIG. 1. Three types of the intermediate states defined in Eq. (10). As explained in the main text, a proton should be excited across at least one shell gap.

calculations. The wave functions of each nucleus are expressed as linear combinations of the possible configurations within a restricted model space referred to as the valence space. As shown in Fig. 1, the proton valence space consists of five orbitals between magic numbers 50 and 82. A single-particle orbital in the spherical harmonic oscillator potential with the spin-orbit splitting is characterized by the number of nodes n, the orbital angular momentum l, and the total angular momentum j. The one-body matrix elements of the NSM operator must vanish unless the initial and final orbitals follow that $\Delta n \leqslant 2$, $\Delta l = 1$, and $\Delta j \leqslant 1$. Since there are no combinations that satisfy all the conditions among the five orbitals in the valence space, we are forced to consider excitations due to the P, T-odd πNN interaction $\widetilde{V}$ across at least one shell gap.

In the present calculations, following the prescription of Ref. [42], the intermediate states $|\psi_n\rangle$ are approximated by one-particle–one-hole excitations from the ground state. The rotational symmetry of the P, T-odd πNN interaction requires the same spin J and the projection M with the ground state. In the one-particle–one-hole approximation, the intermediate states are then expressed with the normalization constants N_n as

$$|\psi_n; JM\rangle = N_n\big[[c^\dagger_{\pi p}\widetilde{c}_{\pi h}]^{(L)}|\psi_0; J\rangle\big]^{(J)}_M, \tag{10}$$

where the square brackets represent the tensor products. An intermediate state is specified by single-particle orbitals p and h coupled to a rank L. The one-particle–one-hole excitations are classified into three types as illustrated in Fig. 1. The one-particle–one-hole excited states in which protons are excited from the valence space across the $Z = 82$ shell gap are referred to as type I. In type II excitations, protons are excited from the core to the valence space. The core orbitals that the excited protons leave should be occupied again in the final state because the core is fully occupied in the shell-model configurations. The excitations from the core across the valence space are referred to as type III. The details of the calculation of the numerator in Eq. (9) are given in Appendix A.

The energy denominators in Eq. (9) are approximated by $E_0 - E_n \approx \varepsilon_h - \varepsilon_p$, where ε_i denotes the single-particle energies in the spherical Nilsson potential. According to Ref. [42], the uncertainty arising from this approximation is roughly estimated as 10%.

In general, the intermediate states approximated by Eq. (10) do not compose the orthogonal basis. The orthogonalization is accomplished by diagonalizing the norm matrix,

$$N_{n'n} = \langle\psi_{n'}; JM|\psi_n; JM\rangle. \tag{11}$$

In the present calculations this procedure varies the NSM coefficients a_T of ^{129}Xe and ^{199}Hg within a few percent.

III. RESULTS

A. ^{129}Xe

For ^{129}Xe, we adopt the valence space that consists of the five orbitals between the magic numbers 50 and 82, $0g_{7/2}$, $1d_{5/2}$, $1d_{3/2}$, $2s_{1/2}$, and $0h_{11/2}$, for both proton and neutron. The ^{129}Xe nucleus has four protons and seven neutron holes in the valence space and the M-scheme dimension reaches 3×10^9. We utilize the shell-model code KSHELL [46] and the Oakforest-PACS supercomputer to perform LSSM calculations throughout this paper.

As an effective interaction, we adopt the SN100PN interaction, which is constructed with a renormalized G matrix derived from the CD-Bonn nucleon-nucleon interaction [47]. The single-particle energies are determined by the low-lying energy levels in ^{133}Sb and ^{131}Sn. The microscopic structure of high-spin states in ^{129}Xe was investigated by LSSM calculations with the SN100PN interaction [48]. We briefly investigate low-spin structure of ^{129}Xe, which is relevant to the accuracy of the NSM.

In order to examine the dependence of the ^{129}Xe NSM on the residual interaction, we employ another well-proven effective interaction. The SNV interaction consists of the SNBG3 interaction for the neutron-neutron part, the N82GYM interaction for the proton-proton part, and the monopole-based universal ($V_{\rm MU}$) interaction for the neutron-proton part [49]. The SNV interaction has been used to investigate nuclear structure of $^{133-134}$Ba and ^{133,135}La [50–52].

Figure 2 shows the calculated excitation energies of the yrast states in comparison with experimental data [53]. The spin and parity $J^\pi = \frac{1}{2}^+$ of the ground state are correctly reproduced with both the effective interactions. Comparing the theoretical results, the positive-parity states with spins $J \geqslant \frac{5}{2}$ are closer to the experimental levels by using the SN100PN interaction. Since the negative-parity states are overbound with the SN100PN interaction, the single-particle energy of the neutron $0h_{11/2}$ orbital might be too low for the neutron-deficient nucleus.

Table I exhibits the magnetic moments of the ground state and the lowest $\frac{3}{2}^+$ and $\frac{11}{2}^-$ states of ^{129}Xe. The spin g factors are attenuated by a factor of 0.7 from the bare values. The same effective g factors $g_{s\nu} = -2.68$ and $g_{s\pi} = 3.91$ were adopted in a PTSM study [54]. The agreement with the experimental values is considerably improved in the present LSSM calculations. In particular the quality of the ground-state wave function would be critical to the accuracy of the NSM coefficients.

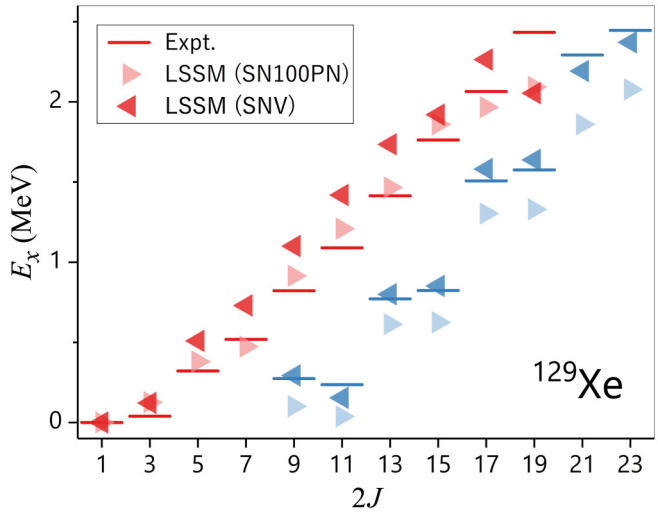

FIG. 2. The energy spectra of ^{129}Xe calculated with the effective interactions SN100PN and SNV. The positive and negative parity states are represented in red and blue, respectively. The experimental levels (Expt.) are extracted from Ref. [53].

Table II summarizes the NSM coefficients a_T of ^{129}Xe. In early studies, Flambaum *et al.* applied the independent particle model (IPM) to calculating the NSM coefficients [35,36]. They employed the Woods-Saxon potential with the spin-orbit correction as a mean field. Dmitriev *et al.* improved the one-body potential by adding a self-consistent mean field obtained from the two-body Landau-Migdal interaction and the Coulomb potential [38]. If the exchange terms in the P, T-odd NN interactions are excluded, the IPM results follow that $a_2 = 2a_0 = 2a_1$ [38] as can be seen in the seventh and eighth rows of Table II. The IPM is helpful to verify the validity of numerical calculations thanks to the simple relation. Moreover, IPM results are expected to be insensitive to the one-body potentials as discussed in the following paragraph.

Flambaum *et al.* adopted the contact P, T-odd NN interaction [35,36], whereas the finite-range P, T-odd πNN interaction has been employed in the recent studies. When the contact interaction was used in Ref. [38] for comparison, the IPM results were increased by a factor of 2 from $a_2 = 2a_0 = 2a_1 = -12$ obtained by using the finite-range interaction. Thus, in the limit of the contact interaction, $m_\pi \to \infty$, the discrepancy between those IPM results is $\sim$10%. This minor difference may come from the improvement of the one-body potential.

TABLE I. Calculated magnetic moments of ^{129}Xe are compared with experimental data (Expt.) and theoretical results in the PTSM. The values are given in units of μ_N.

	$\frac{1}{2}^+_1$ (g.s.)	$\frac{3}{2}^+_1$	$\frac{11}{2}^-_1$
LSSM (SN100PN)	−0.832	0.590	−1.006
LSSM (SNV)	−0.858	0.586	−1.012
Expt. [53]	−0.778	0.58(8)	−0.891
PTSM [54]	−0.268	0.278	−1.13

TABLE II. The NSM coefficients of ^{129}Xe in units of $10^{-2}e$ fm^3. Our final results are given in bold.

	a_0	a_1	a_2
IPM ($m_\pi \to \infty$)	−9.9	−9.9	−19.8
IPM	−4.6	−4.6	−9.2
LSSM (SN100PN, $m_\pi \to \infty$)	−8.7	−8.2	−15.8
LSSM (SNV, $m_\pi \to \infty$)	−8.6	−8.3	−16.2
LSSM (SN100PN)	−3.7	−4.1	−8.0
LSSM (SNV)	**−3.8**	**−4.1**	**−8.1**
IPM ($m_\pi \to \infty$) [35,36]	−11	−11	−22
IPM [38]	−6	−6	−12
RPA [38]	−0.8	−0.6	−0.9
PTSM [41]	0.05	−0.04	0.19
PTSM [42]	0.3	−0.1	0.4

The first two rows of Table II show our IPM results. We construct an artificial configuration in which the proton $0g_{7/2}$ and the neutron $0h_{11/2}$ orbitals are partially occupied and the last neutron occupies the $2s_{1/2}$ orbital. It is confirmed in the present calculations that the IPM results are increased approximately by a factor of 2 in the infinite pion-mass limit. Comparing the first and second rows of Table II with the seventh and eighth rows, respectively, it is found that our IPM results are smaller than the IPM results of the early studies by 10–20 %. The discrepancy could be attributed to the different one-body potentials and occupation probabilities of single-particle orbitals.

The third to sixth rows of Table II show the NSM coefficients by using the wave functions obtained from the LSSM calculations. The configuration mixing reduces the NSM coefficients by factors of 0.8–0.9 from the IPM results. It is noticeable that the results are almost independent of the effective interactions, whereas the overlap probability between the ground-state wave functions obtained by using the SN100PN and SNV interactions is 0.85. On the other hand, those quenching factors are moderate compared with the results in the random phase approximation (RPA) [38] and the pair-truncated shell model (PTSM) [41,42], which are shown in the last three rows.

In the PTSM, nuclear wave functions are expressed as linear combinations of configurations that are made of collective pairs of like nucleons. Such a truncation scheme enables the diagonalization of H_0 even in an extended valence space [41]. In the earlier PTSM study, the valence space is enlarged to contain four proton orbitals, $2p_{1/2}$, $2p_{3/2}$, $1f_{5/2}$, and $1f_{7/2}$, above the present valence space. The obtained excited states with a spin-parity of $\frac{1}{2}^-$ are applied to the intermediate states in Eq. (9). The NSM coefficients are two orders of magnitude smaller than the present LSSM results. This situation could be reasonable because that approximation of the intermediate states exclude the excitations from the core such as type II and type III excitations in Fig. 1. The type I contributions should be suppressed since the proton valence space is almost vacant in ^{129}Xe. In fact, the type I contributions account for less than one-tenth of the NSM coefficients a_T in the present calculations.

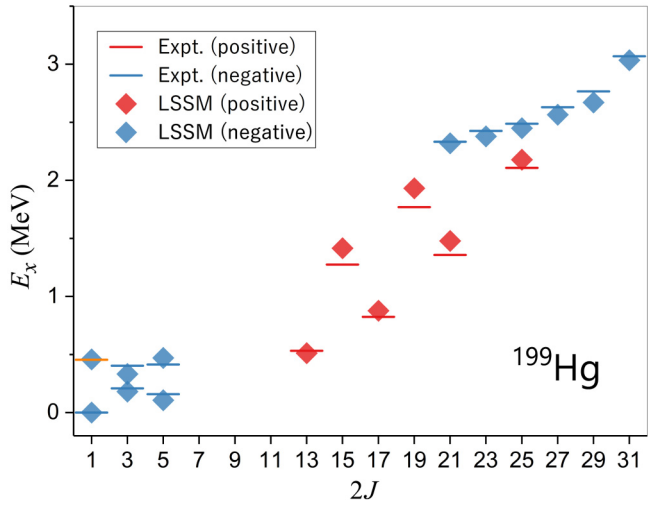

FIG. 3. The energy spectrum of ^{199}Hg. The experimental data are extracted from Ref. [60]. The spin and parity of the experimental level represented in orange are ambiguously assigned $\frac{1}{2}^-$ or $\frac{3}{2}^-$.

In the later PTSM study [42], the valence space is limited to one major shell as the present study, and all the one-particle–one-hole excited states are employed as intermediate states. Although we follow the same prescription, their results are one order of magnitude smaller than the LSSM results. This inconsistency might be attributed to the drastic truncation scheme and the magnetic moment could be important in reducing the uncertainty of the NSM. However, the consistency check of the IPM calculations is indispensable for the comparison between the LSSM and PTSM results. As explained above, our IPM results are effectively consistent with the IPM results in Refs. [35,36,38]. We also confirm that the IPM results for ^{199}Hg differ from those in preceding studies by at most ∼10%. We utilize the same computational code to calculate the NSM coefficients by using the wave functions obtained from the LSSM calculations.

B. ^{199}Hg

We also perform LSSM calculations for ^{199}Hg and neighboring nuclei. The neutron valence space consists of the six orbitals between the magic numbers 82 and 126, $0h_{9/2}$, $1f_{7/2}$, $1f_{5/2}$, $2p_{3/2}$, $2p_{1/2}$, and $0i_{13/2}$. The proton valence space is identical with that of ^{129}Xe. As an effective interaction, we adopt the Kuo-Herling interaction, which was originally developed by the G-matrix approach with the use of the Hamada-Johnston potential [55–57]. Some of the two-body matrix elements were fitted to the experimental data of ^{206}Pb, ^{206}Tl, and ^{206}Hg [58,59].

Figure 3 shows calculated low-lying energy spectrum compared with experimental data. The correct spin and parity of the ground state are reproduced. The second $\frac{1}{2}^-$ state is predicted at 0.458 MeV, which may correspond to the negative parity state discovered in experiment with an excitation energy of 0.455 MeV. In fact a spin-parity of $J^\pi = \frac{1}{2}^-$ is assigned as a strong candidate although $J^\pi = \frac{3}{2}^-$ has not been excluded yet [61–64].

TABLE III. The NSM coefficients of ^{199}Hg in units of $10^{-2}e$ fm^3. Our final results are given in the fourth row.

	a_0	a_1	a_2
IPM ($m_\pi \to \infty$)	7.3	7.3	14.7
IPM	8.4	8.4	16.7
LSSM ($m_\pi \to \infty$)	8.8	9.2	19.0
LSSM	**8.0**	**7.8**	**14.7**
LSSM ($J^\pi = \frac{1}{2}^-_2$)	−0.05	0.4	1.3
IPM ($m_\pi \to \infty$) [36]	8.7	8.7	17.4
IPM ($m_\pi \to \infty$) [37,38]	5.8	5.8	11.6
IPM [37,38]	8.6	8.6	17.2
RPA [37,38]	0.04	5.5	0.9
IPM [39]	9.5	9.5	19.0
QRPA [39]	0.2 ↔ 1.0	5.7 ↔ 9.0	1.1 ↔ 2.5
HFB (SLy4) [40]	1.3	−0.6	2.4
HFB (SkM*) [40]	4.1	−2.7	6.9

Table III exhibits the NSM coefficients of ^{199}Hg. The simple configuration in the IPM is uniquely determined by occupying nucleons from the bottom to the Fermi surface. The last neutron occupies the $2p_{1/2}$ orbital, which gives the correct spin and parity $J^\pi = \frac{1}{2}^-$. The first two rows show the results in the IPM. We confirm the fact that the NSM coefficients are unexpectedly reduced in the infinite pion-mass limit [37,38].

As shown in the fourth row, the LSSM results are quenched by 4–12 % from the IPM evaluations. The present result of a_1 is within the uncertainty estimated in the QRPA calculations with several Skyrme interactions [39]. Although the same Skyrme interactions are employed, the a_1 value is drastically reduced in the fully self-consistent HFB calculations [40]. The results of a_0 and a_2 are rather close to the HFB results, whereas those values are quenched by one order of magnitude in the QRPA calculations.

Here, we present the nuclear spin matrix elements of ^{199}Hg, which are key information on the contribution from the P, T-odd electron-nucleon interaction to the atomic EDM. The spin matrix elements of neutron and proton are computed as $\langle\sigma_{\nu z}\rangle = -0.322$ and $\langle\sigma_{\pi z}\rangle = -0.006$, respectively. Those results support the conclusion from a PTSM calculation [65] that the simple estimate is adequate unless nucleons outside the valence space greatly contribute to the spin matrix elements.

We attempt to exploit a modified Kuo-Herling interaction, which was adjusted further by mainly using high-spin excitation energies of nuclei where the numbers of valence nucleon holes are 2–5 [66]. When the revised effective interaction is employed, the lowest negative parity state of each spin $J \geqslant \frac{21}{2}$ is calculated lower than that with the adopted interaction by ∼0.1 MeV. Moreover, the reduced electric quadrupole transition probability, $B(E2)$, from the 8^+_1 state to the 6^+_1 state in ^{200}Hg is calculated as 7 W.u., which is inconsistent with the experimental value 41(14) W.u. Since the $B(E2; 8^+_2 \to 6^+_1)$ value is calculated as 26 W.u., the lowest 8^+ state in experiment would correspond to the 8^+_2 state. In contrast, low-lying states are little affected by this revision. The NSM coefficients are reduced by less than 2%.

IV. DISCUSSION

In this section, we focus on the serious discrepancies between the theoretical predictions on the NSM coefficients a_T of ^{199}Hg. It was argued in the QRPA study [39] that the neutron excitation from the core plays a crucial role in the destructive interference with a_0 and a_2. This effect is excluded in the present framework owing to the restricted valence space, which might be responsible for the relatively moderate quenching in the LSSM calculations. The P, T-even NN interactions between the present valence space and the core should be treated explicitly in future studies. In contrast, the isovector NSM coefficients a_1 obtained by the QRPA calculations are comparable with IPM results as shown in Table III. The dependence of a_T on the isospin structure of the P, T-odd πNN interaction was explained with the effective potential of the P, T-odd πNN interaction [39]. As can be seen in Eq. (9) of Ref. [31], the effective potential does not suppress the isovector NSM coefficient a_1, but a_0 and a_2. However, the HFB calculations predicted that the isovector NSM coefficient a_1 is much more drastically reduced as shown in Table III. It would be difficult to explain the significant reduction of a_1 on the basis of the effective potential.

We discuss a possible origin of the strong dependence of the NSM coefficients a_T on different nuclear models. In general low-lying excited states of the same spin and parity could be highly mixed, depending on different nuclear models and effective interactions, with the ground state. We pay attention to the second lowest $\frac{1}{2}^-$ state, which is shown in Fig. 3. The NSM coefficients in the $\frac{1}{2}^-_2$ state are given in the fifth row of Table III. It is noticeable that those values are more than one order of magnitude smaller than those in the ground state. Thus, if the $\frac{1}{2}^-_2$ state is mixed with the ground state to some extent in other models, the NSM coefficients will be considerably reduced from the desirable values in the ground state, which are comparable with the IPM evaluation.

In order to understand the strong quenching of the NSM coefficients in the $\frac{1}{2}^-_2$ state, we analyze the microscopic nuclear structure. A significant difference between the lowest two $\frac{1}{2}^-$ states is the purity of the $\nu p_{1/2} \otimes 0^+_1$ configuration, where the ground state of ^{200}Hg is denoted by 0^+_1. In the ground state of ^{199}Hg, the spectroscopic factor defined by Eq. (B1) for the neutron $2p_{1/2}$ orbital is calculated as $S = 0.93$, which accounts for 41% of the sum-rule value in Eq. (B2). This value is consistent with experimental results of $S = 0.70(35)$ [63,67] and $S = 1.10$ [68]. Since the $\nu p_{1/2} \otimes 0^+_1$ configuration is similar to the simple configuration of the IPM, it is reasonable that the quenching of the NSM coefficients is moderate in the ground state. In contrast, the spectroscopic factor is calculated as $S = 0.05$ in the $\frac{1}{2}^-_2$ state. It is remarkable that the ratio of the spectroscopic factors of the lowest two $\frac{1}{2}^-$ states is comparable with the ratio of the results of each NSM coefficient.

It has been demonstrated that experimental energy spectra of several nuclei in the vicinity of ^{208}Pb are systematically reproduced with the Kuo-Herling interaction and its modified version [66,69–76]. Those agreements ensure the validity of the effective interaction and the ordering of the lowest two $\frac{1}{2}^-$ states. It is known that electromagnetic properties can be used to confirm such assignments thanks to the sensitivity to details of nuclear structure [77]. The magnetic moment of the ground state in ^{199}Hg was precisely measured as $0.506\mu_N$ [60]. In the LSSM calculation, the magnetic moment is calculated with effective spin g factors quenched by a factor of 0.8 as $0.459\mu_N$. The theoretical magnetic moment of the $\frac{1}{2}^-_2$ state is $0.612\mu_N$. Since these theoretical values of the $\frac{1}{2}^-_1$ and $\frac{1}{2}^-_2$ states are close to each other, we cannot conclude their correspondence to the experimental ground state utilizing the magnetic moment.

TABLE IV. $B(E2)$ values in units of W.u. The effective charges $e_\pi = 1.5e$ and $e_\nu = 0.8e$ are determined by fitting $B(E2)$ values in even-even Hg isotopes.

^{199}Hg	Expt.	LSSM	LSSM ($\to \frac{1}{2}^-_2$)
$\frac{5}{2}^-_1 \to \frac{1}{2}^-_1$	17.6 (3)	8.7	2.8
$\frac{5}{2}^-_2 \to \frac{1}{2}^-_1$	4.8 (10)	14.2	0.9
sum	22.4 (10)	22.9	3.7
$\frac{3}{2}^-_1 \to \frac{1}{2}^-_1$	16.1 (11)	7.2	8.1
$\frac{3}{2}^-_2 \to \frac{1}{2}^-_1$	8.1 (20)	10.4	3.1
sum	24.2 (20)	17.6	11.2
^{200}Hg	Expt.	LSSM	
$2^+_1 \to 0^+_1$	24.57 (22)	22.7	

Table IV exhibits $B(E2)$ values between low-lying states in ^{199}Hg. The effective charges $e_\pi = 1.5e$ and $e_\nu = 0.8e$ are determined so that the experimental $B(E2)$ values of ^{200,202,204,206}Hg are reproduced in the LSSM calculations. The $B(E2)$ enhancement in low-lying excited states of odd-mass nuclei such as ^{199}Hg was explained with the core excitation model [78]. In this model, the lowest $\frac{3}{2}^-$ and $\frac{5}{2}^-$ states and the second lowest $\frac{3}{2}^-$ and $\frac{5}{2}^-$ states are interpreted as admixtures of the $\nu p_{1/2} \otimes 2^+_1$ and $\nu p_{1/2} \otimes 2^+_2$ configurations [79,80]. However, the present LSSM calculations suggest that the single-particle excitations to the neutron $1f_{5/2}$ and $2p_{3/2}$ orbitals are more important than the core excitation to the 2^+_2 state of ^{200}Hg. For example, the lowest two $\frac{5}{2}^-$ states mainly consist of the $\nu p_{1/2} \otimes 2^+_1$ and $\nu f_{5/2} \otimes 0^+_1$ configurations as illustrated in Fig. 4. Thus, the $\frac{5}{2}^-$ states inherit the collective nature of the 2^+_1 state of ^{200}Hg and the $B(E2; \frac{5}{2}^- \to \frac{1}{2}^-_1)$ values are enhanced between the $\nu p_{1/2} \otimes 2^+_1$ configuration in the $\frac{5}{2}^-$ states and the $\nu p_{1/2} \otimes 0^+_1$ configuration in the ground state. As shown in Table IV, the summed $B(E2)$ values in ^{199}Hg are very similar to the $B(E2; 2^+_1 \to 0^+_1)$ value in ^{200}Hg. If the lowest two $\frac{1}{2}^-$ states were inverted from their experimental order, the summed $B(E2)$ value of the ground state should be suppressed.

Figure 5 shows the accumulation of the isovector NSM coefficient a_1 in the ground state. The type II contribution is suppressed in ^{199}Hg in contrast to ^{129}Xe because the proton valence space is almost fully occupied. The type I and type III contributions form drastic increases at 7 and 24 MeV. The NSM operator demands one or three harmonic oscillator excitation, which corresponds to each characteristic excitation

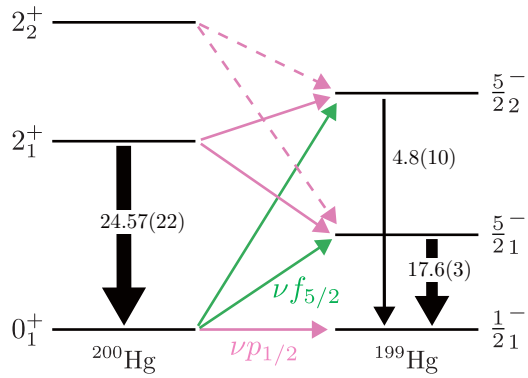

FIG. 4. The predicted main configurations of low-lying states in ^{199}Hg. The magenta and green arrows represent the coupling of the neutron $2p_{1/2}$ and $1f_{5/2}$ orbitals to ^{200}Hg, respectively. The dashed arrows mean that the $\nu p_{1/2} \otimes 2_2^+$ configuration is a minor component in the $\frac{5}{2}^-$ states. The experimental $B(E2)$ values are given in W.u.

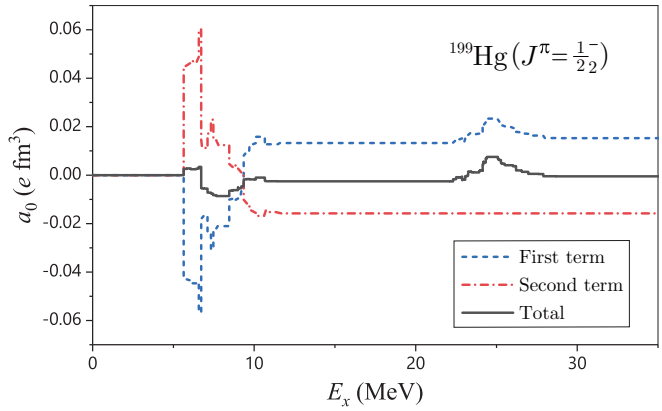

FIG. 6. The integrated NSM coefficient a_0 of ^{199}Hg in the $\frac{1}{2}^-_2$ state. The contributions from the first term and the second term of the NSM operator are shown in dashed line and dash-dotted line, respectively.

energy. As shown in Fig. 5 in Ref. [39], such two bumps are also found in the QRPA calculations. As mentioned above, the residual interactions between the valence space and the core are not included explicitly in the LSSM calculations. The drawback of the present framework appears in the plateau region between two bumps in Fig. 5. Although, the onset of the second bump is more gentle in the QRPA calculations [39], one can find that the two bumps are separated by an almost flat section except for the result with SIII Skyrme interaction.

Figure 6 shows the accumulation of isoscalar NSM coefficient a_0 in the $\frac{1}{2}^-_2$ state. It is found that the significant reduction results from the cancellation between the contributions from the first and second terms of the NSM operator. The same feature is found in a_0 obtained in the QRPA calculations as shown in Fig. 6 of Ref. [39].

V. CONCLUSION

We have calculated the NSMs of ^{129}Xe and ^{199}Hg using the microscopic wave functions obtained from LSSM calculations. The quenching of the NSM coefficients due to the residual interactions is moderate compared with the results in the RPA, the QRPA, the fully self-consistent HFB theory, and the pair-truncated shell model except for the isovector NSM coefficient a_1 of ^{199}Hg obtained from the RPA and QRPA calculations. It has been found that the NSM coefficients in the $\frac{1}{2}^-_2$ state of ^{199}Hg are one order of magnitude smaller than the results in the ground state. Consequently, if the $\frac{1}{2}^-_2$ state is mixed to the ground state by using different nuclear models or effective interactions, the NSM coefficients could be considerably reduced.

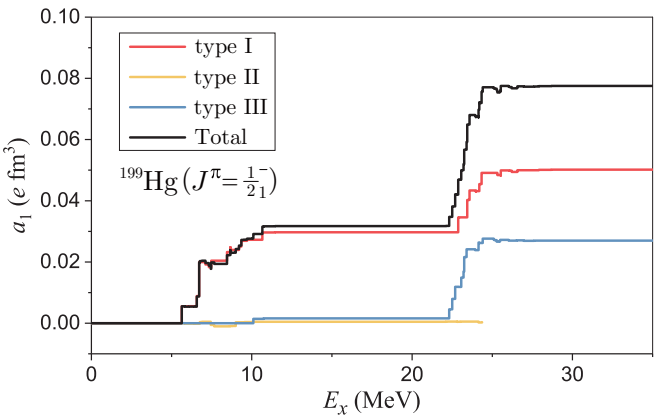

FIG. 5. The integrated NSM coefficient a_1 of ^{199}Hg in the ground state ($J^\pi = \frac{1}{2}^-_1$). The horizontal axis represents the excitation energy of the intermediate states.

The reliability of our calculations is limited by the one-particle–one-hole approximation to the intermediate states, whereas the residual correlations might be crucial in the strong quenching of the NSM coefficients. The residual interactions between the present valence space and the core should be considered in future studies.

Our final result for ^{129}Xe is given in units of e fm^3 as

$$S(^{129}\mathrm{Xe}) = -0.038 g\bar{g}^{(0)} - 0.041 g\bar{g}^{(1)} - 0.082 g\bar{g}^{(2)}. \quad (12)$$

The ^{129}Xe atomic EDM induced by the NSM has been calculated in the Dirac-Fock method [81,82], the coupled-perturbed-Hartree-Fock method [83], the RPA [81,82], and the relativistic coupled-cluster (RCC) model [84]. In the recent study using the RCC model, the electric dipole polarizability of the atomic system is accurately reproduced with a discrepancy of 2% [85]. The state-of-the-art atomic calculation presented $d_A\,[e\,\mathrm{cm}]/S\,[e\,\mathrm{fm}^3] = 3.20 \times 10^{-18}$. Combining the atomic factor and our result, the ^{129}Xe atomic EDM is predicted in units of e cm as

$$d(^{129}\mathrm{Xe}) = -1.7 \times 10^{-18}\bar{g}^{(0)} - 1.8 \times 10^{-18}\bar{g}^{(1)} - 3.7 \times 10^{-18}\bar{g}^{(2)}, \quad (13)$$

where $g_{\pi NN} = 14.11$ is adopted [86]. The upper bound in experiment is $d(^{129}\mathrm{Xe}) < 1.4 \times 10^{-27} e\,\mathrm{cm}$ [30].

The atomic factor of ^{199}Hg has been calculated in the Dirac-Fock method [81,82], the multiconfiguration Dirac-Hartree-Fock method [87,88], the RPA [81,82], the configu-

ration interaction method [82], and the RCC model [89–92]. The latest study based on the RCC model presented $d_A\,[e\,\mathrm{cm}]/S\,[e\,\mathrm{fm}^3] = -1.77 \times 10^{-17}$. In this model, the electric dipole polarizability is well reproduced. Combining the atomic factor and our result, which is given in units of $e\,\mathrm{fm}^3$ as

$$S(^{199}\mathrm{Hg}) = 0.079\bar{gg}^{(0)} + 0.075\bar{gg}^{(1)} + 0.143\bar{gg}^{(2)}, \quad (14)$$

the atomic EDM is calculated in units of $e\,\mathrm{cm}$ as

$$d(^{199}\mathrm{Hg}) = -2.0 \times 10^{-17}\bar{g}^{(0)} - 1.9 \times 10^{-17}\bar{g}^{(1)} - 3.7 \times 10^{-17}\bar{g}^{(2)}, \quad (15)$$

whereas the current limit is given in 95% C.L. as $d(^{199}\mathrm{Hg}) < 7.4 \times 10^{-30} e\,\mathrm{cm}$ [26].

ACKNOWLEDGMENTS

This research was supported by MEXT and JICFuS as post-K priority issue 9 (hp180179, hp190160) and Program for Promoting Researches on the Supercomputer "Fugaku" (Simulation for basic science: from fundamental laws of particles to creation of nuclei). It was also supported by a KAKENHI grant (17K05433). The numerical calculation was performed mainly on the Oakforest-PACS supercomputer for Multidisciplinary Computational Sciences Project of Tsukuba University (xg18i035). We acknowledge Cenxi Yuan for the discussions about the Kuo Herling interaction, Yutaka Utsuno for the discussions about the spectroscopic factor, Naotaka Yoshinaga, and Koji Higashiyama for helpful discussions.

APPENDIX A: MATRIX ELEMENTS

The NSM operator and the P, T-odd πNN interaction are expressed as

$$S_z = \sum_{ij} s_{ij} c_i^\dagger c_j, \quad \widetilde{V} = \sum_{i<j} \sum_{k<l} \widetilde{v}_{ijkl} c_i^\dagger c_j^\dagger c_l c_k, \quad (A1)$$

where s_{ij} and $\widetilde{v}_{ijkl}$ are the one-body matrix elements of S_z and the two-body matrix elements of $\widetilde{V}$, respectively. A subscript denotes a single-particle state and the z component of isospin. The many-body matrix elements are calculated as follows.

As explained in Sec. II, there are three types of the intermediate states. In type I one-particle–one-hole excitations, protons in the valence space are excited to higher orbitals across the $Z = 82$ shell gap. In type II, protons are excited from the core to the valence space. In type III, protons are excited from the core across the valence space.

For type I excitations, the many-body matrix elements in Eq. (9) can be reduced to

$$\begin{aligned}
&\langle\psi_0|S_z|\psi_n\rangle\langle\psi_n|\widetilde{V}|\psi_0\rangle \\
&= \langle\psi_0|\left(\sum_{i'j'} s_{i'j'} c_{i'}^\dagger a_{j'}\right) a_p^\dagger c_h|\psi_0\rangle \\
&\quad \times \langle\psi_0|c_h^\dagger a_p\left(\sum_{ij}\sum_{k\leqslant l} \widetilde{v}_{ijkl} a_i^\dagger c_j^\dagger c_l c_k\right)|\psi_0\rangle \\
&= \sum_{i'j}\sum_{k\leqslant l} s_{i'p}\widetilde{v}_{pjkl}\langle\psi_0|c_{i'}^\dagger c_h|\psi_0\rangle\langle\psi_0|c_h^\dagger c_j^\dagger c_l c_k|\psi_0\rangle, \quad (A2)
\end{aligned}$$

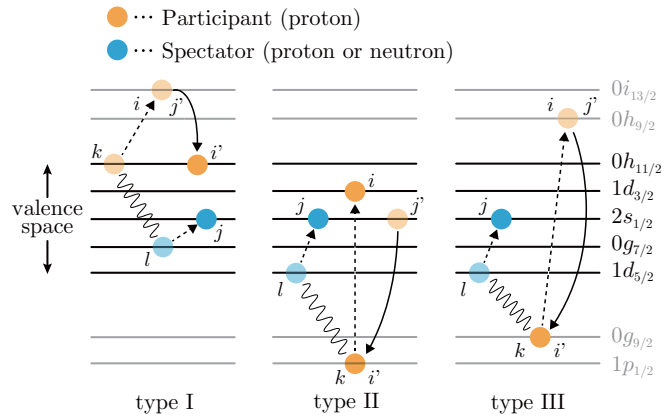

FIG. 7. A schematic diagram illustrating the one-body and two-body transitions through the NSM operator (solid arrows) and the P, T-odd πNN interaction (dashed arrows), respectively. The P, T-odd πNN interaction represented by a wavy line should excite a proton, which is referred to as a participant, across at least one shell gap. The participant proton interacts with a "spectator", which is a proton or neutron. Although the spectators are shown in the valence space, nucleons in the core also behave as spectators that remain in the same orbitals ($j = l$). The indices indicating single-particle states correspond to those in Eqs. (A2)–(A4).

where $a_i^\dagger$ is the proton creation operator of a single-particle orbital higher than the valence space. Here, $a_i|\psi_0\rangle = 0$ is used. For type II excitations, we have

$$\begin{aligned}
&\langle\psi_0|S_z|\psi_n\rangle\langle\psi_n|\widetilde{V}|\psi_0\rangle \\
&= \langle\psi_0|\left(\sum_{i'j'} s_{i'j'} b_{i'} c_{j'}\right) c_p^\dagger b_h^\dagger|\psi_0\rangle \\
&\quad \times \langle\psi_0|b_h c_p\left(\sum_{i\leqslant j}\sum_{kl} \widetilde{v}_{ijkl} c_i^\dagger c_j^\dagger c_l b_k^\dagger\right)|\psi_0\rangle \\
&= \sum_{i\leqslant j}\sum_{j'l} s_{hj'}\widetilde{v}_{ijhl}\langle\psi_0|c_{j'}c_p^\dagger|\psi_0\rangle\langle\psi_0|c_p c_i^\dagger c_j^\dagger c_l|\psi_0\rangle, \quad (A3)
\end{aligned}$$

where the proton-hole creation operator of a core orbital $b_k^\dagger$ follows $b_k|\psi_0\rangle = 0$. For type III excitations, we have

$$\begin{aligned}
&\langle\psi_0|S_z|\psi_n\rangle\langle\psi_n|\widetilde{V}|\psi_0\rangle \\
&= \langle\psi_0|\left(\sum_{i'j'} s_{i'j'} b_{i'} a_{j'}\right) a_p^\dagger b_h^\dagger|\psi_0\rangle \\
&\quad \times \langle\psi_0|b_h a_p\left(\sum_{ijkl} \widetilde{v}_{ijkl} a_i^\dagger c_j^\dagger c_l b_k^\dagger\right)|\psi_0\rangle \\
&= \sum_{jl} s_{hp}\widetilde{v}_{pjhl}\langle\psi_0|c_j^\dagger c_l|\psi_0\rangle. \quad (A4)
\end{aligned}$$

The one-body and two-body matrix elements in Eqs. (A2)–(A4) are computed by using the ground-state wave functions $|\psi_0\rangle$ obtained from the LSSM calculations. Figure 7 shows a schematic explanation of the contribution to the NSM from each type of the intermediate states.

APPENDIX B: SPECTROSCOPIC FACTOR

The spectroscopic factors for the single-neutron stripping reactions of ^{199}Hg are defined by [93]

$$S_k(n_i, J_i; n_f, J_f) = \frac{1}{2J_f + 1} |\langle {}^{200}\mathrm{Hg}(n_f, J_f) || c_k^\dagger || {}^{199}\mathrm{Hg}(n_i, J_i) \rangle|^2, \quad \text{(B1)}$$

where k is the single-particle orbital of the neutron and (n, J) denotes the nth lowest state with the spin J. In general C^2 is multiplied, where C is the Clebsch-Gordan coefficient of isospin. In the present calculations of ^{199}Hg, it follows $C = 1$. The spectroscopic factors satisfy sum rules as

$$\sum_{n_f J_f} (2J_f + 1) S_k = (2J_i + 1)\big[(2j + 1) - N_k^i(n_i, J_i)\big], \quad \text{(B2)}$$

where N_k^i and N_k^f are the occupation numbers of a single-particle orbital k in the initial and final states, respectively.

TABLE V. The sign conventions of F_T and the isospin z component of the neutron. $F_T = -1$ means the sign convention is opposite to ours.

	F_0	F_1	F_2	$\langle \tau_z \rangle_n$
Engel *et al.* [39,40] and this paper	+1	+1	+1	+1
Domitriev *et al.* [37,38]	−1	+1	+1	(−1)
Yoshinaga *et al.* [41,42]	+1	−1	+1	+1

APPENDIX C: SIGN CONVENTIONS OF THE P, T-ODD πNN INTERACTION

Table V summarizes the sign conventions of F_T in Eq. (4) and the isospin z component of the neutron, which is involved in the sign of $\widetilde{V}_1$ in Eq. (3), adopted in preceding works and ours. We infer the isospin z component of the neutron $\langle \tau_z \rangle_n = -1$ adopted by Dmitriev *et al.* from Eq. (7) in Ref. [38]. This assumption is also supported by the consistency of the IPM results of a_1 as shown in Tables II and III. In this paper we follow the conventions of Refs. [39,40].

[1] P. G. H. Sandars, The electric dipole moment of an atom, Phys. Lett. **14**, 194 (1965).

[2] P. G. H. Sandars, Enhancement factor for the electric dipole moment of the valence electron in an alkali atom, Phys. Lett. **22**, 290 (1966).

[3] P. G. H. Sandars and R. M. Sternheimer, Electric-dipole-moment enhancement factor for the thallium atom, and a new upper limit on the electric dipole moment of the electron, Phys. Rev. A **11**, 473 (1975).

[4] H. S. Nataraj, B. K. Sahoo, B. P. Das, and D. Mukherjee, Intrinsic Electric Dipole Moments of Paramagnetic Atoms: Rubidium and Cesium, Phys. Rev. Lett. **101**, 033002 (2008).

[5] H. S. Nataraj, B. K. Sahoo, B. P. Das, and D. Mukherjee, Reappraisal of the Electric Dipole Moment Enhancement Factor for Thallium, Phys. Rev. Lett. **106**, 200403 (2011).

[6] D. Mukherjee, B. K. Sahoo, H. S. Nataraj, and B. P. Das, Relativistic coupled cluster (RCC) computation of the electric dipole moment enhancement factor of francium due to the violation of time reversal symmetry, J. Phys. Chem. A **113**, 12549 (2009).

[7] J. S. M. Ginges and V. V. Flambaum, Violations of fundamental symmetries in atoms and tests of unification theories of elementary particles, Phys. Rep. **397**, 63 (2004).

[8] M. C. Weisskopf, J. P. Carrico, H. Gould, E. Lipworth, and T. S. Stein, Electric Dipole Moment of the Cesium Atom. A New Upper Limit to the Electric Dipole Moment of the Electron, Phys. Rev. Lett. **21**, 1645 (1968).

[9] S. A. Murthy, D. Krause, Z. L. Li, and L. R. Hunter, New Limits on the Electron Electric Dipole Moment from Cesium, Phys. Rev. Lett. **63**, 965 (1989).

[10] E. D. Commins, S. B. Ross, D. DeMille, and B. C. Regan, Improved experimental limit on the electric dipole moment of the electron, Phys. Rev. A **50**, 2960 (1994).

[11] B. C. Regan, E. D. Commins, C. J. Schmidt, and D. DeMille, New Limit on the Electron Electric Dipole Moment, Phys. Rev. Lett. **88**, 071805 (2002).

[12] A. Uchiyama, K. Harada, T. Inoue, H. Kawamura, K. Tanaka, M. Itoh, T. Aoki, A. Hatakeyama, Y. Takahashi, and Y. Sakemi, Development of a dual isotope co-magnetometer using laser cooled rubidium toward electron electric dipole moment measurement using francium, J. Phys.: Conf. Ser. **1206**, 012008 (2019).

[13] J. Baron, W. C. Campbell, D. DeMille, J. M. Doyle, G. Gabrielse, Y. V. Gurevich, P. W. Hess, N. R. Hutzler, E. Kirilov, I. Kozyryev, B. R. O'Leary, C. D. Panda, M. F. Parsons, E. S. Petrik, B. Spaun, A. C. Vutha, and A. D. West (ACME Collaboration), Order of magnitude smaller limit on the electric dipole moment of the electron, Science **343**, 269 (2014).

[14] V. Andreev, D. G. Ang, D. DeMille, J. M. Doyle, G. Gabrielse, J. Haefner, N. R. Hutzler, Z. Lasner, C. Meisenhelder, B. R. O'Leary, C. D. Panda, A. D. West, E. P. West, and X. Wu (ACME Collaboration), Improved limit on the electric dipole moment of the electron, Nature **562**, 355 (2018).

[15] V. V. Flambaum and I. B. Khriplovich, New bounds on the electric dipole moment of the electron and on T-odd electron-nucleon coupling, Zh. Eksp. Teor. Fiz. **89**, 1505 (1985).

[16] A.-M. Mårtensson-Pendrill and P. Öster, Calculations of atomic electric dipole moments, Phys. Scr. **36**, 444 (1987).

[17] L. I. Schiff, Measurability of nuclear electric dipole moments, Phys. Rev. **132**, 2194 (1963).

[18] C.-P. Liu and J. Engel, Schiff screening of relativistic nucleon electric-dipole moments by electrons, Phys. Rev. C **76**, 028501 (2007).

[19] C.-P. Liu, M. J. Ramsey-Musolf, W. C. Haxton, R. G. E. Timmermans, and A. E. L. Dieperink, Atomic electric dipole moments: The Schiff theorem and its corrections, Phys. Rev. C **76**, 035503 (2007).

[20] S. K. Lamoreaux, J. P. Jacobs, B. R. Heckel, F. J. Raab, and N. Fortson, New Constraints on Time-Reversal Asymmetry from a Search for a Permanent Electric Dipole Moment of ^{199}Hg, Phys. Rev. Lett. **59**, 2275 (1987).

[21] J. P. Jacobs, W. M. Klipstein, S. K. Lamoreaux, B. R. Heckel, and E. N. Fortson, Testing Time-Reversal Symmetry Using ^{199}Hg, Phys. Rev. Lett. **71**, 3782 (1993).

[22] J. P. Jacobs, W. M. Klipstein, S. K. Lamoreaux, B. R. Heckel, and E. N. Fortson, Limit on the electric-dipole moment of ^{199}Hg using synchronous optical pumping, Phys. Rev. A **52**, 3521 (1995).

[23] M. V. Romalis, W. C. Griffith, J. P. Jacobs, and E. N. Fortson, New Limit on the Permanent Electric Dipole Moment of ^{199}Hg, Phys. Rev. Lett. **86**, 2505 (2001).

[24] W. C. Griffith, M. D. Swallows, T. H. Loftus, M. V. Romalis, B. R. Heckel, and E. N. Fortson, Improved Limit on the Permanent Electric Dipole Moment of ^{199}Hg, Phys. Rev. Lett. **102**, 101601 (2009).

[25] M. D. Swallows, T. H. Loftus, W. C. Griffith, B. R. Heckel, E. N. Fortson, and M. V. Romalis, Techniques used to search for a permanent electric dipole moment of the ^{199}Hg atom and the implications for *CP* violation, Phys. Rev. A **87**, 012102 (2013).

[26] B. Graner, Y. Chen, E. G. Lindahl, and B. R. Heckel, Reduced Limit on the Permanent Electric Dipole Moment of ^{199}Hg, Phys. Rev. Lett. **116**, 161601 (2016); **119**, 119901(E) (2017).

[27] T. G. Vold, F. J. Raab, B. Heckel, and E. N. Fortson, Search for a Permanent Electric Dipole Moment on the ^{129}Xe Atom, Phys. Rev. Lett. **52**, 2229 (1984).

[28] M. A. Rosenberry and T. E. Chupp, Atomic Electric Dipole Moment Measurement Using Spin Exchange Pumped Masers of ^{129}Xe and ^{3}He, Phys. Rev. Lett. **86**, 22 (2001).

[29] F. Allmendinger, I. Engin, W. Heil, S. Karpuk, H.-J. Krause, B. Niederländer, A. Offenhäusser, M. Repetto, U. Schmidt, and S. Zimmer, Measurement of the permanent electric dipole moment of the ^{129}Xe atom, Phys. Rev. A **100**, 022505 (2019).

[30] N. Sachdeva, I. Fan, E. Babcock, M. Burghoff, T. E. Chupp, S. Degenkolb, P. Fierlinger, S. Haude, E. Kraegeloh, W. Kilian, S. Knappe-Grüneberg, F. Kuchler, T. Liu, M. Marino, J. Meinel, K. Rolfs, Z. Salhi, A. Schnabel, J. T. Singh, S. Stuiber, W. A. Terrano, L. Trahms, and J. Voigt, New Limit on the Permanent Electric Dipole Moment of ^{129}Xe using ^{3}He Comagnetometry and Squid Detection, Phys. Rev. Lett. **123**, 143003 (2019).

[31] J. Engel, M. Bender, J. Dobaczewski, J. H. de Jesus, and P. Olbratowski, Time-reversal violating Schiff moment of ^{225}Ra, Phys. Rev. C **68**, 025501 (2003).

[32] J. Dobaczewski, J. Engel, M. Kortelainen, and P. Becker, Correlating Schiff Moments in the Light Actinides with Octupole Moments, Phys. Rev. Lett. **121**, 232501 (2018).

[33] R. H. Parker, M. R. Dietrich, M. R. Kalita, N. D. Lemke, K. G. Bailey, M. Bishof, J. P. Greene, R. J. Holt, W. Korsch, Z.-T. Lu, P. Mueller, T. P. O'Connor, and J. T. Singh, First Measurement of the Atomic Electric Dipole Moment of ^{225}Ra, Phys. Rev. Lett. **114**, 233002 (2015).

[34] M. Bishof, R. H. Parker, K. G. Bailey, J. P. Greene, R. J. Holt, M. R. Kalita, W. Korsch, N. D. Lemke, Z.-T. Lu, P. Mueller, T. P. O'Connor, J. T. Singh, and M. R. Dietrich, Improved limit on the ^{225}Ra electric dipole moment, Phys. Rev. C **94**, 025501 (2016).

[35] V. V. Flambaum, I. B. Khriplovich, and O. P. Sushkov, Limit on the Constant of T-Nonconserving Nucleon-Nucleon Interaction, Phys. Lett. B **162**, 213 (1985).

[36] V. V. Flambaum, I. B. Khriplovich, and O. P. Sushkov, On the P-and T-nonconserving nuclear moments, Nucl. Phys. A **449**, 750 (1986).

[37] V. F. Dmitriev and R. A. Sen'kov, P-and T-violating Schiff moment of the mercury nucleus, Phys. At. Nucl. **66**, 1940 (2003).

[38] V. F. Dmitriev, R. A. Sen'kov, and N. Auerbach, Effects of core polarization on the nuclear Schiff moment, Phys. Rev. C **71**, 035501 (2005).

[39] J. H. de Jesus and J. Engel, Time-reversal-violating Schiff moment of ^{199}Hg, Phys. Rev. C **72**, 045503 (2005).

[40] S. Ban, J. Dobaczewski, J. Engel, and A. Shukla, Fully self-consistent calculations of nuclear Schiff moments, Phys. Rev. C **82**, 015501 (2010).

[41] N. Yoshinaga, K. Higashiyama, R. Arai, and E. Teruya, Nuclear Schiff moments for the lowest $1/2^+$ states in Xe isotopes, Phys. Rev. C **87**, 044332 (2013); **89**, 069902(E) (2014).

[42] E. Teruya, N. Yoshinaga, K. Higashiyama, and K. Asahi, Effects of particle-hole excitations to nuclear Schiff moments in Xe isotopes, Phys. Rev. C **96**, 015501 (2017).

[43] V. Spevak, N. Auerbach, and V. V. Flambaum, Enhanced T-odd, P-odd electromagnetic moments in reflection asymmetric nuclei, Phys. Rev. C **56**, 1357 (1997).

[44] I. B. Khriplovich and S. Lamoreaux, *CP Violation without Strangeness: Electric Dipole Moments of Particles, Atoms, and Molecules* (Springer-Verlag, Berlin, Heidelberg, 1997).

[45] W. Dekens, J. de Vries, J. Bsaisou, W. Bernreuther, C. Hanhart, U.-G. Meißner, A. Nogga, and A. Wirzba, Unraveling models of CP violation through electric dipole moments of light nuclei, J. High Energy Phys. 07 (2014) 069.

[46] N. Shimizu, T. Mizusaki, Y. Utsuno, and Y. Tsunoda, Thick-restart block Lanczos method for large-scale shell-model calculations, Comput. Phys. Commun. **244**, 372 (2019).

[47] B. A. Brown, N. J. Stone, J. R. Stone, I. S. Towner, and M. Hjorth-Jensen, Magnetic moments of the 2_1^+ states around ^{132}Sn, Phys. Rev. C **71**, 044317 (2005).

[48] L. Kaya, A. Vogt, P. Reiter, M. Siciliano, B. Birkenbach, A. Blazhev, L. Coraggio, E. Teruya, N. Yoshinaga, K. Higashiyama, K. Arnswald, D. Bazzacco, A. Bracco, B. Bruyneel, L. Corradi *et al.*, High-spin structure in the transitional nucleus ^{131}Xe: Competitive neutron and proton alignment in the vicinity of the $N = 82$ shell closure, Phys. Rev. C **98**, 014309 (2018).

[49] Y. Utsuno, T. Otsuka, N. Shimizu, M. Honma, T. Mizusaki, Y. Tsunoda, and T. Abe, Recent shell-model results for exotic nuclei, EPJ Web Conf. **66**, 02106 (2014).

[50] L. Kaya, A. Vogt, P. Reiter, M. Siciliano, N. Shimizu, Y. Utsuno, H.-K. Wang, A. Gargano, L. Coraggio, N. Itaco, K. Arnswald, D. Bazzacco, B. Birkenbach, A. Blazhev, A. Bracco *et al.*, Isomer spectroscopy in ^{133}Ba and high-spin structure of ^{134}Ba, Phys. Rev. C **100**, 024323 (2019).

[51] M. S. R. Laskar, S. Saha, R. Palit, S. N. Mishra, N. Shimizu, Y. Utsuno, E. Ideguchi, Z. Naik, F. S. Babra, S. Biswas, S. Kumar, S. K. Mohanta, C. S. Palshetkar, P. Singh, and P. C. Srivastava, g-factor measurement of the 2738 keV isomer in ^{135}La, Phys. Rev. C **99**, 014308 (2019).

[52] M. S. R. Laskar, R. Palit, S. N. Mishra, N. Shimizu, Y. Utsuno, E. Ideguchi, U. Garg, S. Biswas, F. S. Babra, R. Gala, C. S. Palshetkar, and Z. Naik, Structure of the $11/2^-$ isomeric state in ^{133}La, Phys. Rev. C **101**, 034315 (2020).

[53] B. S. J. Timar, Z. Elekes, Nuclear data sheets for $A = 129$, Nucl. Data Sheets **121**, 143 (2014).

[54] K. Higashiyama and N. Yoshinaga, Pair-truncated shell-model analysis of nuclei around mass 130, Phys. Rev. C **83**, 034321 (2011); **89**, 049903(E) (2014).

[55] T. T. S. Kuo and G. Herling, US Naval Research Laboratory Report No. 2258, 1971 (unpublished).

[56] G. H. Herling and T. T. S. Kuo, Two-particle states in ^{210}Pb, ^{210}Bi and ^{210}Po with realistic forces, Nucl. Phys. A **181**, 113 (1972).

[57] J. B. Mcgrory and T. T. S. Kuo, Shell model calculations of two to four identical "particle" systems near ^{208}Pb, Nucl. Phys. A **247**, 283 (1975).

[58] J. Blomqvist, L. Rydström, R. J. Liotta, and C. Pomar, Multiplet structure in ^{205}Pb and ^{203}Pb, Nucl. Phys. A **423**, 253 (1984).

[59] L. Rydström, J. Blomqvist, R. J. Liotta, and C. Pomar, Structure of proton-deficient nuclei near ^{208}Pb, Nucl. Phys. A **512**, 217 (1990).

[60] B. Singh, Nuclear data sheets for $A = 199$, Nucl. Data Sheets **108**, 79 (2007).

[61] B. Jung and J. Svedberg, The electron spectrum of $_{81}$Tl^{199}, Nucl. Phys. **20**, 630 (1960).

[62] R. W. Bauer, L. Grodzins, and H. H. Wilson, Decay of Tl^{199} and Au^{199}, Phys. Rev. **128**, 694 (1962).

[63] G. J. Mathews, F. M. Bernthal, and J. D. Immele, Population of levels in ^{199}Hg following ^{199}Tl decay and intermediate coupling calculations for ^{199}Hg, Phys. Rev. C **11**, 587 (1975).

[64] M. A. Lone, E. D. Earle, and G. A. Bartholomew, Resonance neutron capture in ^{198,199,201}Hg, Nucl. Phys. A **243**, 413 (1975).

[65] K. Yanase, N. Yoshinaga, K. Higashiyama, and N. Yamanaka, Electric dipole moment of ^{199}Hg atom from P, CP-odd electron-nucleon interaction, Phys. Rev. D **99**, 075021 (2019).

[66] B. Szpak, K. H. Maier, A. S. Smolkowska, B. Fornal, R. Broda, M. P. Carpenter, N. Cieplicka, R. V. F. Janssens, W. Królas, T. Pawłat, J. Wrzesiński, and S. Zhu, Yrast structure of the two-proton- and three-neutron-hole nucleus ^{203}Hg from the decay of a $53/2^+$ isomer, Phys. Rev. C **83**, 064315 (2011).

[67] R. A. Moyer, Deuteron-induced reactions on the even-even isotopes of mercury, Phys. Rev. C **5**, 1678 (1972).

[68] M. Vergnes, S. Grafeuille, G. Rotbard, G. Berrier-Ronsin, J. Vernotte, J. M. Maison, S. Fortier, R. Tamisier, P. Van Isacker, and J. Jolie, Transfer in the light Hg isotopes and the U(6/12) models, Phys. Rev. C **31**, 2071 (1985).

[69] J. Wrzesiński, G. J. Lane, K. H. Maier, R. V. F. Janssens, G. D. Dracoulis, R. Broda, A. P. Byrne, M. P. Carpenter, R. M. Clark, M. Cromaz, B. Fornal, T. Lauritsen, A. O. Macchiavelli, M. Rejmund, B. Szpak, K. Vetter, and S. Zhu, High-spin yrast structure of ^{204}Hg from the decay of a four-hole, 22^+ isomer, Phys. Rev. C **92**, 044327 (2015).

[70] B. Silvestre-Brac and J. P. Boisson, Shell model calculations in the lead region: ^{205}Hg, ^{205}Tl, ^{211}Po, and ^{211}Bi, Phys. Rev. C **24**, 717 (1981).

[71] R. Broda, K. H. Maier, B. Fornal, J. Wrzesiński, B. Szpak, M. P. Carpenter, R. V. F. Janssens, W. Królas, T. Pawłat, and S. Zhu, High-spin states and isomers in the one-proton-hole and three-neutron-hole ^{204}Tl isotope, Phys. Rev. C **84**, 014330 (2011).

[72] M. Y. Chen, S. C. Cheng, W. Y. Lee, A. M. Rushton, and C. S. Wu, Resonance processes and nuclear excitation in muonic ^{205}Tl, Nucl. Phys. A **181**, 25 (1972).

[73] N. Cieplicka-Orynczak, C. Michelagnoli, S. Leoni, B. Fornal, G. Benzoni, A. Blanc, S. Bottoni, F. C. L. Crespi, L. W. Iskra, M. Jentschel *et al.*, The Low-spin structure of ^{206}Tl studied by γ-ray spectroscopy from thermal neutron capture reaction, Acta Phys. Pol. B **49**, 561 (2018).

[74] Z. Podolyák, G. F. Farrelly, P. H. Regan, A. B. Garnsworthy, S. J. Steer, M. Górska, J. Benlliure, E. Casarejos, S. Pietri, J. Gerl *et al.*, Proton-hole excitation in the closed shell nucleus ^{205}Au, Phys. Lett. B **672**, 116 (2009).

[75] Z. Podolyák, S. J. Steer, S. Pietri, M. Górska, P. H. Regan, D. Rudolph, A. B. Garnsworthy, R. Hoischen, J. Gerl, H. J. Wollersheim *et al.*, Structure of neutron-rich nuclei around the $N = 126$ closed shell; the yrast structure of ^{205}Au$_{126}$ up to spin-parity $I^\pi = (19/2^+)$, Euro. Phys. J. A **42**, 489 (2009).

[76] S. J. Steer, Z. Podolyák, S. Pietri, M. Górska, P. H. Regan, D. Rudolph, E. Werner-Malento, A. B. Garnsworthy, R. Hoischen, J. Gerl, H. J. Wollersheim, K. H. Maier, H. Grawe, F. Becker, P. Bednarczyk, L. Cáceres, P. Doornenbal, H. Geissel, J. Grebosz, A. Kelic, I. Kojouharov, N. Kurz, F. Montes, W. Prokopowicz, T. Saito, H. Schaffner, S. Tashenov, A. Heinz, M. Pfützner, T. Kurtukian-Nieto, G. Benzoni, A. Jungclaus, D. L. Balabanski, C. Brandau, B. A. Brown, A. M. Bruce, W. N. Catford, I. J. Cullen, Z. Dombrádi, M. E. Estevez, W. Gelletly, G. Ilie, J. Jolie, G. A. Jones, M. Kmiecik, F. G. Kondev, R. Krücken, S. Lalkovski, Z. Liu, A. Maj, S. Myalski, S. Schwertel, T. Shizuma, P. M. Walker, and O. Wieland, Single-particle behavior at $N = 126$: Isomeric decays in neutron-rich ^{204}Pt, Phys. Rev. C **78**, 061302(R) (2008).

[77] G. Neyens, M. Kowalska, D. Yordanov, K. Blaum, P. Himpe, P. Lievens, S. Mallion, R. Neugart, N. Vermeulen, Y. Utsuno, and T. Otsuka, Measurement of the Spin and Magnetic Moment of ^{31}Mg: Evidence for a Strongly Deformed Intruder Ground State, Phys. Rev. Lett. **94**, 022501 (2005).

[78] A. de Shalit, Core excitations in nondeformed, odd-A, nuclei, Phys. Rev. **122**, 1530 (1961).

[79] R. Kalish, R. R. Borchers, and H. W. Kugel, Revised level scheme of ^{199}Hg following Coulomb excitation, Nucl. Phys. A **161**, 637 (1970).

[80] R. Vianden and K. Krien, Quadrupole moment of the $\frac{5}{2}^-$, 134 keV state in ^{197}Hg, Nucl. Phys. A **277**, 442 (1977).

[81] V. A. Dzuba, V. V. Flambaum, J. S. M. Ginges, and M. G. Kozlov, Electric dipole moments of Hg, Xe, Rn, Ra, Pu, and TlF induced by the nuclear Schiff moment and limits on time-reversal violating interactions, Phys. Rev. A **66**, 012111 (2002).

[82] V. A. Dzuba, V. V. Flambaum, and S. G. Porsev, Calculation of (P, T)-odd electric dipole moments for the diamagnetic atoms ^{129}Xe, ^{171}Yb, ^{199}Hg, ^{211}Rn, and ^{225}Ra, Phys. Rev. A **80**, 032120 (2009).

[83] Y. Singh, B. K. Sahoo, and B. P. Das, *Ab initio* determination of the P- and T-violating coupling constants in atomic Xe by the relativistic-coupled-cluster method, Phys. Rev. A **89**, 030502(R) (2014); **90**, 039903(E) (2014).

[84] A. Sakurai, B. K. Sahoo, K. Asahi, and B. P. Das, Relativistic many-body theory of the electric dipole moment of ^{129}Xe and its implications for probing new physics beyond the standard model, Phys. Rev. A **100**, 020502(R) (2019).

[85] A. Sakurai, B. K. Sahoo, and B. P. Das, Electric dipole polarizability of ^{129}Xe using the relativistic coupled-cluster and the normal coupled-cluster methods, Phys. Rev. A **97**, 062510 (2018).

[86] N. Yamanaka and E. Hiyama, Standard model contribution to the electric dipole moment of the deuteron, ^{3}H, and ^{3}He nuclei, J. High Energy Phys. 02 (2016) 067.

[87] L. Radžiūtė, G. Gaigalas, P. Jönsson, and J. Bieroń, Multiconfiguration Dirac-Hartree-Fock calculations of atomic electric dipole moments of ^{225}Ra, ^{199}Hg, and ^{171}Yb, Phys. Rev. A **90**, 012528 (2014).

[88] L. Radžiūtė, G. Gaigalas, P. Jönsson, and J. Bieroń, Electric dipole moments of superheavy elements: A case study on copernicium, Phys. Rev. A **93**, 062508 (2016).

[89] K. V. P. Latha, D. Angom, B. P. Das, and D. Mukherjee, Probing *CP* Violation with the Electric Dipole Moment of Atomic Mercury, Phys. Rev. Lett. **103**, 083001 (2009); **103**, 119902(E) (2009); **115**, 059902(E) (2015).

[90] Y. Singh and B. K. Sahoo, Rigorous limits on the hadronic and semileptonic *CP*-violating coupling constants from the electric dipole moment of ^{199}Hg, Phys. Rev. A **91**, 030501(R) (2015).

[91] B. K. Sahoo, Improved limits on the hadronic and semihadronic *CP* violating parameters and role of a dark force carrier in the electric dipole moment of ^{199}Hg, Phys. Rev. D **95**, 013002 (2017).

[92] B. K. Sahoo and B. P. Das, Relativistic Normal Coupled-Cluster Theory for Accurate Determination of Electric Dipole Moments of Atoms: First Application to the ^{199}Hg Atom, Phys. Rev. Lett. **120**, 203001 (2018).

[93] P. Ring and P. Schuck, *The Nuclear Many-Body Problem* (Springer-Verlag, Berlin, Heidelberg, 1980).